ACS APPLIED ENERGY MATERIALS

www.acsaem.org
Article

Ionic Liquid and Ionic Plastic Crystal Electrolytes Compatible with Silver Positive Electrode for Fast Charge/Discharge Fluoride-Shuttle Batteries at Room Temperature

Takayuki Yamamoto,* Kazuhiko Matsumoto, Rika Hagiwara, and Toshiyuki Nohira*

Cite This: *ACS Appl. Energy Mater.* 2025, 8, 108−121
Read Online

ABSTRACT: Fluoride shuttle batteries (FSBs) have been acclaimed as prospective candidates for next-generation energy applications for their superior energy densities that transcend state-of-the-art lithium-ion battery performances. Despite these prospects, their practical deployment has been heavily afflicted by the scarcity of energy materials that facilitate fast charge−discharge capabilities and prolonged cycle life for room-temperature operations. In a bid to expand the materials available for FSB operations, this study comprehensively investigates the performance and reaction mechanisms of a silver positive electrode working in fluorohydrogenate ionic liquid (FHIL) and fluorohydrogenate ionic plastic crystal (FHIPC) electrolytes at 298 K. The silver electrode working in the $[C_2C_1im][(FH)_{2.3}F]$ (C_2C_1im = 1-ethyl-3-methylimidazolium) FHIL electrolyte exhibits unprecedented active material utilization ratios that surpass any conventional materials. The superior rate capability and cycling properties of the silver electrode are ascribed to two-step reactions that form Ag_2F and AgF phases during the charge−discharge processes. A comparison between the performance of electrodes with differently sized silver particles accredit the high rate performance to the electron conductive Ag and Ag_2F in the electrode as well as the F^- ion conductive AgF. In an attempt to exploit the operational advantages of electrolyte solidification, we investigate the performance an FSB employing the $[C_1C_1pyrr][(FH)_{1.9}F]$ (C_1C_1pyrr = *N*,*N*-dimethylpyrrolidinium) FHIPC as both the electrolyte and an F^- ion conductive binder in the composite electrode. Employing a silver composite electrode with the FHIPC binder is observed to improve the active material utilization ratios during operations. Herein, we unveil a streamlined fabrication process of the electrodes where the prescribed components are prepared at room temperature without the electrolyte impregnation step that requires elevated temperatures. This work not only highlights silver metal as an eligible positive electrode material for room-temperature FSBs but also provides invaluable insights for the development and optimization of high-performance fluoride-based electrochemical systems.

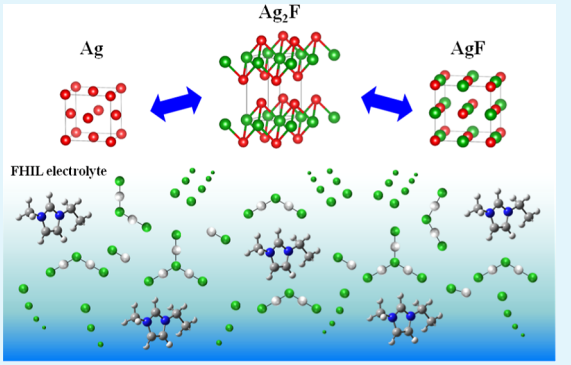

KEYWORDS: *fluoride-shuttle battery, ionic liquid, ionic plastic crystal, ion conductive binder, silver, positive electrode*

1. INTRODUCTION

The global proliferation of electric vehicles marks a paradigm shift from traditional fossil fuels, signaling the promising transition toward a society sustained by renewable energy sources such as solar and wind power. To fulfill these evolving energy demands, lithium-ion batteries (LIBs) have gained widespread utility due to their relatively high energy densities, which are primarily achieved through topotactic reactions. While LIBs continue to outperform other commercialized batteries in applications such as portable electronics and smart grid systems, their energy densities are still limited to the 250−300 W·h kg^{-1} range, making them insufficient for the projected growth in electric vehicles.[1] The search for future energy storage solutions has driven explorations into alternative concepts like metal−air batteries[2,3] and multivalent ion batteries, including magnesium[4] and calcium[5] batteries to achieve high theoretical energy densities.

Over the past decade, fluoride-shuttle batteries (FSBs) have emerged as prospective electrochemical storage devices with superior energy densities and improved safety for next-generation applications. This novel class of batteries, which operates through fluoride ion transport between the positive and negative electrodes,[6−8] employs metals (M or M′) or their fluorides (MF_x or $M'F_y$) as active materials to facilitate charge−discharge operations that entail the following reactions

$$\text{positive electrode: } M + xF^- \rightleftharpoons MF_x + xe^- \quad (1)$$

Received: August 7, 2024
Revised: November 26, 2024
Accepted: November 27, 2024
Published: December 16, 2024

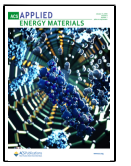

$$\text{negative electrode: } (x/y)\mathrm{M'F}_y + xe^- \rightleftharpoons (x/y)\mathrm{M'} + xF^- \quad (2)$$

During electrochemical operations, the positive electrode active materials, i.e., copper (Cu), bismuth (Bi), tin (Sn), and lead (Pb), facilitate multielectron reactions that endow FSBs with high theoretical capacities (Table S1) that even surpass those of the state-of-the-art LIBs currently available.

The progress achieved in FSBs so far is rooted in multifaceted contributions made over the years. In early stage FSB studies, inorganic solid electrolytes such as PbF_2[9−13] and $La_{1-x}Ba_xF_{3-x}$ ($0 \le x \le 1$)[14] were found to have moderate fluoride ion conductivities, establishing their feasibility for constructing reversible galvanic cells. In a report by Anji Reddy and Fichtner et al. in 2011, a cerium metal (Ce) negative electrode used alongside various positive electrodes (CuF_2, BiF_3, $KBiF_4$, and SnF_2) in the $La_{0.9}Ba_{0.1}F_{2.9}$ electrolyte showed improved charge−discharge performances at 423 K,[6] due to the high utilization ratios of most of the active materials which were noted to exceed 60%. Since then, interest in this class of batteries has prompted comprehensive studies into various solid-state electrolytes for FSBs,[6,15−21] although most reports have shown that high temperatures above 353 K are required for sufficient performance.

The high temperatures required for FSB operations present a major challenge to their practical utilization, inspiring tremendous efforts to develop room-temperature FSBs—particularly those using liquid or polymer-type electrolytes.[22−34] For instance, in noteworthy contributions by Konishi et al., CsF/glyme-based electrolytes optimized by adding anion acceptors were found to enhance the performance of BiF_3 and PbF_2 positive electrodes in their first three charge−discharge cycles.[23−25] In another study, Okazaki et al. successfully ascertained the reversible fluorination/defluorination behavior of bismuth positive electrodes in TFSA-based ionic liquid electrolytes (TFSA = bis(trifluoromethylsulfonyl)-amide).[27] Davis et al. also demonstrated the electrochemical viability of an electrolyte composed of *N*,*N*,*N*-trimethyl-*N*-neopentylammonium fluoride salt dissolved into bis(2,2,2-trifluoroethyl)ether solvent through charge−discharge tests performed using copper, lead, and cerium metal electrodes.[28] Further, some recent studies developed water-in-salt electrolytes with wide electrochemical windows,[31,32] and attempted to construct Pb/CuF_2 full cells with alcoholic electrolytes containing CsF.[33,34] These studies represent only a few among many other contributions made to enhance the performance of electrolytes for room temperature operations. However, it should be noted that in most studies, the utilization ratios of active materials were either found to be much lower than the theoretical capacities or could not be well evaluated.

In a bid to advance this research field, our group has extensively investigated the use of fluorohydrogenate ionic liquids (FHILs) as electrolytes on account of their high ionic conductivities and fluorination capabilities in the presence of fluorohydrogenate anions, $[(FH)_nF]^-$.[35−42] In one of our developmental studies, we formulated an exemplar FHIL: $[C_2C_1im][(FH)_{2.3}F]$ (C_2C_1im = 1-ethyl-3-methylimidazolium) with a high ionic conductivity of 100 mS cm^{-1} at 298 K, being a key indicator of its eligibility as an electrolyte.[36] These outstanding physicochemical properties originates from the nature of fluorohydrogenate anions.[38] We previously reported that fast HF exchange between $[(FH)_nF]^-$ anions occurs in FHILs [e.g., $(FH)_2F^- + HF \rightleftharpoons (FH)_3F^-$]. The exchange medium HF acts as a dielectric spacer and lowers the Coulombic interaction between cations and anions, leading to extremely high ionic conductivity at room temperature. In addition, the transference number of fluorohydrogenate anion in $[C_2C_1im][(FH)_{2.3}F]$ based on the ratio of diffusion coefficients is approximately 0.58 at 298 K.[39]

In a subsequent study, we established that this FHIL could facilitate high utilization ratios of copper-based active materials when employed as an FSB electrolyte.[41,42] Here, a CuF_2 positive electrode in the $[C_2C_1im][(FH)_{2.3}F]$ FHIL electrolyte at 298 K, exhibited initial discharge (defluorination) and charge (fluorination) capacities of 517 and 475 mAh $(g\text{-}CuF_2)^{-1}$ that correspond to 98% and 90% of the theoretical capacity [528 mAh $(g\text{-}CuF_2)^{-1}$], respectively.[41] Further, we reported the performance of copper metal positive electrodes in the same FHIL at 298 K, where reversible capacities exceeding 430 mAh $(g\text{-}Cu)^{-1}$ were obtained from the initial two cycles.[42] However, the reversible capacities of the copper-based positive electrodes have been noted to rapidly decrease to less than half within 10 cycles. Furthermore, their sluggish kinetics limit the charge−discharge current rates to below 0.1C (10 h-charge and discharge), only allowing moderate capacity utilization.

As with most electrochemical storage systems, the choice of positive electrode plays an essential role in establishing the performance of FSBs. A summary of potential active materials for FSB positive electrodes and their theoretical capacities is provided in Table S1. Among the listed candidate active materials, silver manifests the lowest theoretical capacity [248 mAh $(g\text{-}Ag)^{-1}$] when a one-electron reaction is assumed. However, according to thermodynamic calculations,[43] the theoretical redox potential of AgF/Ag is significantly higher than those of CuF_2/Cu, BiF_3/Bi, SnF_2/Sn, and PbF_2/Pb by 0.61, 0.96, 1.18, and 1.34 V, respectively, making silver a unique and attractive positive electrode candidate for FSBs. Silver monofluoride (AgF) has previously been reported as a dopant of PbF_2-based solid-state electrolyte.[12] However, the compound was found to manifest poor performance when used as a positive electrode in galvanic cells.[11] As such, the electrochemical fluorination and defluorination of silver metal remains underexplored with only a few reports available. Kawasaki et al. reported the electrochemical fluorination and defluorination of several metals, including silver, in a lactone-based liquid electrolyte.[44] In their study, charge−discharge tests were conducted using a silver plate electrode, after which the formation of AgF was confirmed by X-ray diffraction. However, the utilization ratio of the silver active material and the details pertaining to the reaction mechanism were not reported. In another study, Yokoyama et al. utilized an AgF/Ag redox couple for fluoride ion-sensing techniques in organic solvent (propylene carbonate) electrolytes owing to the reversibility of the reaction.[45]

Among the common avenues for improving battery practicality, the solidification of electrolytes is considered a propitious strategy for improving operational safety. Even so, the adoption of inorganic solid electrolytes is often encumbered by the performance challenges associated with their poor electrode/electrolyte interfaces.[46] Thus, we focused on fluorohydrogenate ionic plastic crystals (FHIPCs) due to their high ionic conductivities and good plasticity that enables the formation of improved electrode/electrolyte interfaces. We have applied FHIPCs to electrochemical capacitors and

https://doi.org/10.1021/acsaem.4c02021
ACS Appl. Energy Mater. 2025, 8, 108−121

succeeded the construction of high performance all solid-state electrochemical capacitors utilizing $[C_1C_1pyrr][(FH)_2F]$ FHIPC (C_1C_1pyrr = *N*,*N*-dimethylpyrrolidinium) as an electrolyte,[47] which shows a reasonably high ionic conductivity of 10.3 mS cm^{-1} at 298 K.[48] As with the case of FHIL, fast HF exchange among fluorohydrogenate anions at neighboring sites is considered to be responsible for the significantly high ionic conductivity in the plastic crystalline solid electrolyte.[48] Despite these prospects, the use of IPCs as FSB electrolytes remain unexplored with no report available to the best of our knowledge. It is worth noting that the adoption of FHIPCs in FSBs is not limited to electrolyte utility. These materials are known for their excellent adhesivity which opens them for use as F^- ion conductive binders in the development of electrochemical components.

In the present report, we elucidate the electrochemical performance of a silver electrode working in FHIL and FHIPC electrolytes through a series of analyses involving cyclic voltammetry, charge−discharge tests including rate capability and cycle performance, and GITT test. The underlying fluorination and defluorination reactions are assessed through X-ray diffraction and a combination of microscopic techniques such as scanning electron microscopy and transmission electron microscopy. This work presents a detailed discussion based on experimental data and thermodynamic calculations to explicate the fundamental mechanisms governing the performance of the silver electrode in the present electrolytes and explore potential avenues for performance and practicality improvements for FSBs.

2. EXPERIMENTAL SECTION

2.1. Materials and Cell Construction. All materials were handled under a dehydrated and deoxygenated argon atmosphere. The fluorohydrogenate ionic liquids ($[C_2C_1im][(FH)_{2.3}F]$ and $[C_2C_1pyrr][(FH)_{2.3}F]$) and their precursors ($[C_2C_1im]Cl$ and $[C_2C_1pyrr]Cl$) were purchased from Morita Chemical Industries Co., Ltd. and Yoyulabo Co., Ltd., respectively. The fluorohydrogenate ionic plastic crystal, $[C_1C_1pyrr][(FH)_{1.9}F]$, was prepared via the method prescribed in our previous studies.[48,49]

All the electrochemical measurements were conducted using three-electrode cells (EC Frontier Co., Ltd.), as illustrated in Figure S1. Silver composite films embedded on platinum mesh current collectors were employed as the working electrodes (denoted as silver electrodes), CuF_2−Cu mixed electrodes as the reference electrodes, and AgF−Ag mixed electrodes as the counter electrodes. The potentials were described with respect to the redox potential couple of CuF_2/Cu couple. The cell construction procedures applied for the cells using the FHIL electrolytes ($[C_2C_1im][(FH)_{2.3}F]$ and $[C_2C_1pyrr][(FH)_{2.3}F]$) were different from those with the FHIPC electrolyte ($[C_1C_1pyrr][(FH)_{1.9}F]$), as detailed below.

2.1.1. FHIL Electrolytes. Silver metal powder with different particle sizes (Aldrich, 150 nm, purity 99%; or Kojundo Chemical Laboratory, 1 μm, purity 99.9%), acetylene black (AB; Strem Chemicals), and polytetrafluoroethylene (PTFE; Aldrich) were used to fabricate the silver composite films for the working electrodes. The composite films were prepared by mixing and grinding the powders of silver, AB, and PTFE in the weight ratios of 60:20:20 to produce smaller silver particles, and 80:10:10 to form larger silver particles. The CuF_2−Cu mixed electrodes were fabricated by mixing and grinding CuF_2 powder (Alfa Acer, purity 99.5%), copper metal powder (Aldrich, 60−80 nm), AB, and PTFE in a weight ratio of 40:30:15:15. The AgF−Ag mixed electrodes were made from a mixture of anhydrous AgF powder (Kojundo Chemical Laboratory), silver metal powder (150 nm), AB, and PTFE ground in a weight ratio of 45:35:10:10. A three-ply PTFE filter (Omnipore, Millipore, thickness: 65 μm, average pore diameter: 0.45 μm, porosity: 80%) was used as a separator for all cells. All electrodes and PTFE filters were impregnated with the electrolyte before cell assembly.

2.1.2. FHIPC Electrolyte. We adopted two preparation methods for silver working electrodes, i.e., conventional impregnation method and F^- conductive binder method. In the former case (conventional impregnation method), a silver electrode consisting of silver (150 nm), AB, and PTFE in the weight ratio of 60:20:20 was impregnated with the electrolyte at temperatures just above the melting point (T_m = 338 K) for 1 h. After assembling the cell at room temperature, the cell was warmed at 323 K for 1 h prior to the electrochemical measurements. The CuF_2−Cu reference electrodes and the AgF−Ag counter electrodes used in this case were fabricated using the same procedures employed for the FHIL-electrolyte cells, and these electrodes and separators were impregnated with the FHIPC electrolyte at ca. 343 K (a temperature slightly above the melting point of the FHIPC).

The latter case of cell construction involved the use of the $[C_1C_1pyrr][(FH)_{1.9}F]$ FHIPC as a F^- ion conductive binder. Silver powder (150 nm), AB, PTFE, and FHIPC were mixed in the weight ratio of 50:15:10:25 in an agate mortar, and pressed onto a platinum mesh to fabricate the working electrode with a F^- ion conductive binder. Similarly, the reference and counter electrodes were also fabricated by mixing the prescribed ingredients with the FHIPC. The weight compositions were CuF_2/Cu/AB/PTFE/FHIPC = 35:25:15:10:15 for reference electrodes and AgF/Ag/AB/PTFE/FHIPC = 40:30:10:10:10 for counter electrodes. In this cell construction case, only the separators were impregnated with the FHIPC electrolyte at temperatures slightly above 343 K in advance. The electrode fabrication and cell construction were performed at room temperature, and charge−discharge tests were started without any prior warming step.

2.2. Analysis. Cyclic voltammetry and charge−discharge tests were conducted using electrochemical measurement apparatus (HZ-7000 or HZ-Pro, Hokuto Denko Corp.) at 298 or 273 K. For the cyclic voltammetry measurements of the silver electrodes, the potentials were swept in the potential range of 0.1−1.1 V vs CuF_2/Cu at scan rates of 0.02 or 10 mV s^{-1}. The cutoff potentials for the charge−discharge tests were set at 0.1 and 1.1 V vs CuF_2/Cu.

The galvanostatic intermittent titration technique (GITT) was conducted in accordance with the following procedure below:

(1) Galvanostatic electrolysis was performed at a current density of 12.4 mA $(g\text{-}Ag)^{-1}$ for 2 h (i.e., 24.8 mA h $(g\text{-}Ag)^{-1}$).
(2) The open-circuit potential was monitored for 3 h. The final potential of this step was regarded as the relaxed open-circuit potential value.
(3) Steps 1 and 2 were repeated 10 times in total until the potential reached 1.1 V during charging and 0.1 V during the discharging (vs CuF_2/Cu) in step 1.

To identify the phases present in the silver metal electrodes before and after the charge−discharge tests, X-ray diffraction (XRD) analysis was performed using an X-ray diffractometer [Ultima IV, Rigaku Co.; Cu Kα radiation (λ = 1.5418 Å)] equipped with a 1D high-speed detector (D/teX Ultra, Rigaku Co.) and a nickel filter. The morphological changes of the silver electrode were analyzed using a field emission scanning electron microscope (FE-SEM; SU-6600, Hitachi) equipped with an energy-dispersive X-ray spectroscope (EDX; EMAX x-act, Horiba). The local crystal evolution was detected via transmission electron microscope (TEM; JEM-2010F or JEM-2100F, JEOL) equipped with an EDX (JED-2300T SSD, JEOL) under liquid nitrogen cooling (~123 K). Prior to the TEM observation, the silver electrodes were processed using a focused ion and electron beam system (nano DUE'T NB5000, Hitachi) under liquid nitrogen cooling (~173 K). Before these analyses, the electrochemical cells were disassembled, and the residual electrolytes on the silver electrode surfaces were removed by soaking the samples in dehydrated and deoxidized ethanol (water content <10 ppm, oxygen content <1 ppm; Wako Pure Chemical Industries, Ltd.). Here, the materials were handled in an argon-filled glovebox. Finally, the samples were transferred to apparatuses without air exposure.

https://doi.org/10.1021/acsaem.4c02021
ACS Appl. Energy Mater. 2025, 8, 108−121

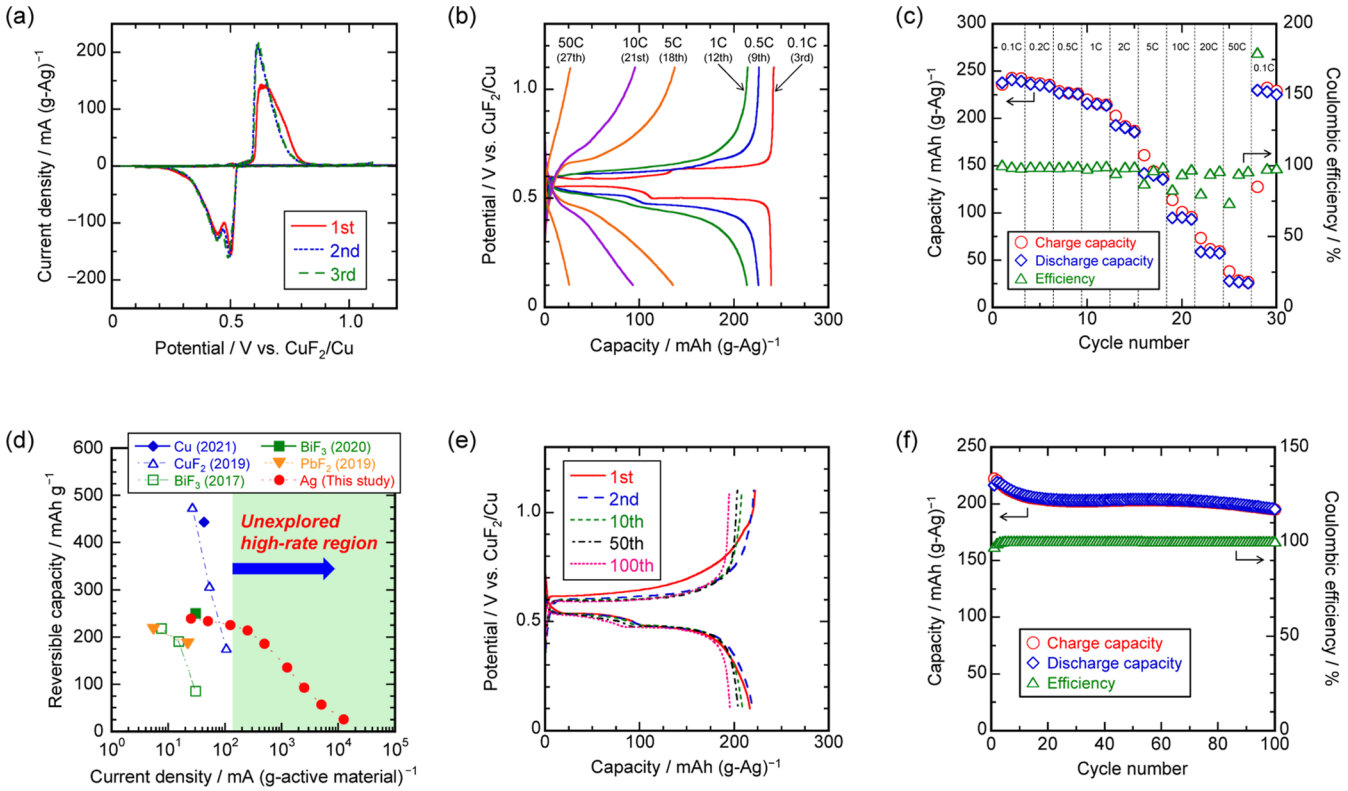

Figure 1. (a) Cyclic voltammograms of a silver electrode (Ag: 150 nm) in $[C_2C_1im][(FH)_{2.3}F]$ ionic liquid at 298 K. Scan rate: 0.02 mV s^{-1}. Rest potential: 0.51 V vs CuF_2/Cu. (b) Charge−discharge curves of a silver electrode (Ag: 150 nm) in $[C_2C_1im][(FH)_{2.3}F]$ ionic liquid at 298 K at varying charge−discharge current rates. The cycle numbers (in parentheses) and the corresponding current rates are provided above the charge−discharge curves, and (c) the cycling properties depicting the capacities and Coulombic efficiencies from the rate capability test. (d) Performance comparison for selected composite-type positive electrodes for room-temperature FSB operations. The plotted points are based on data reported in previous studies.[23,25,29,41,42] (e) Charge−discharge curves of a silver electrode (Ag: 150 nm) in $[C_2C_1im][(FH)_{2.3}F]$ ionic liquid cycled at 298 K at a current rate of 0.5C [=124 mA (g-Ag)$^{-1}$], and (f) the cycling properties depicting the capacities and Coulombic efficiencies from the cyclability test.

The solubility of AgF in the ionic liquid electrolyte was determined through inductively coupled plasma atomic emission spectroscopy (ICP-AES; SPECTRO BLUE, Hitachi) under the following procedure: First, the AgF powder was added into the $[C_2C_1im][(FH)_{2.3}F]$ ionic liquid at 298 K and stirred for 24 h. The residual powder was then separated by filtration, and the resultant liquid was diluted by adding a 0.1 mol dm^{-3} nitric acid aqueous solution. Finally, the solution was subjected to ICP-AES measurements to determine the concentration of silver in the solution.

3. RESULTS AND DISCUSSION

3.1. Charge−Discharge Performance of Silver Positive Electrode in FHIL. The fundamental electrochemical behavior of the silver metal electrode in the FHIL electrolyte were investigated through cyclic voltammetry measurements conducted on a silver composite film (Ag particle size: 150 nm) in the $[C_2C_1im][(FH)_{2.3}F]$ FHIL electrolyte at a scan rate of 0.02 mV s^{-1} at room temperature (~298 K). As shown in Figure 1a, the current profile obtained in the first cycle during the positive potential scan from the rest potential (~0.51 V vs CuF_2/Cu) reveals that oxidation currents significantly increase around 0.6 V, forming a large prominent peak in the 0.6−0.8 V potential region. The peak appears to have a shoulder at around 0.75 V, pointing to the occurrence of a multistep reaction in the silver electrode. After switching to the negative potential scan at 1.1 V, the reduction currents also sharply increase from 0.53 V and develop two peaks that seemingly correspond to the multistep reaction detected in the oxidation currents. The reaction potentials observed here are close to the redox potentials calculated for the AgF/Ag with respect to the CuF_2/Cu reference electrode (see Table S1), suggesting that the oxidation and reduction currents correspond to the fluorination and defluorination of silver, respectively. The second cycle measurements provide sharper oxidation currents around 0.6 V, implying that facile reaction pathways have been established in the silver electrode. In addition, these sharper peaks suggest that the equilibrium potentials of the multiple reactions are rather close to each other, apparently forming a single current peak. Moreover, the potential polarization in the fluorination process seems smaller than that in the defluorination process because the reduction currents are obviously composed of two peaks, which will be discussed in the later section. The current profile obtained from the negative potential scan in this cycle notably resembles the one from the first cycle. Further, the voltammograms obtained from the third cycle nearly overlap with those from the previous cycle (second cycle), indicating that the silver electrode facilitates stable redox reactions in this potential range.

To ascertain the charge−discharge behavior of the silver positive electrode, its rate capability test was conducted in the $[C_2C_1im][(FH)_{2.3}F]$ FHIL electrolyte at 298 K, as shown in Figure 1b,c. For initial three cycles conducted at the current rate of 0.1C [=24.8 mA (g-Ag)$^{-1}$], the silver electrode delivers charge−discharge capacities of approximately 240 mAh (g-

https://doi.org/10.1021/acsaem.4c02021
ACS Appl. Energy Mater. 2025, 8, 108−121

Ag)$^{-1}$ that are comparable to the theoretical capacity of silver [=248 mAh (g-Ag)$^{-1}$]. Both the charge and the discharge processes are characterized by two potential plateaus corresponding to the CV results. The charge−discharge mechanism will be discussed in detail later in this report. Notably, the reversible capacities gradually decrease when the current density is increased in the subsequent cycles. However, the silver positive electrode retains a discharge capacity of 214 mAh (g-Ag)$^{-1}$, which is commensurate with 86% of the theoretical capacity and 89% of the capacity at the current rate of 0.1C, even at the high current rate of 1C (12th cycle).

In one of our previous studies on copper-based positive electrodes for FSBs,[41] the CuF_2 positive electrode cycled at the current rate of 0.05C [=26.4 mA (g-CuF_2)$^{-1}$] exhibited an initial discharge capacity of over 470 mAh (g-CuF_2)$^{-1}$ in $[C_2C_1im][(FH)_{2.3}F]$ FHIL, corresponding to ca. 90% of the theoretical capacity [=528 mAh (g-CuF_2)$^{-1}$]. However, increasing the current density to 0.1C and 0.2C resulted in diminished reversible capacities of 308 and 177 mAh (g-CuF_2)$^{-1}$, respectively; commensurate to 58% and 34% of the theoretical capacity.[41] In another report, we found that the copper metal electrode in the $[C_2C_1im][(FH)_{2.3}F]$ FHIL yielded reversible capacities of ca. 440 mAh (g-Cu)$^{-1}$ at the current rate of 0.05C [=42.2 mA (g-Cu)$^{-1}$], corresponding to only 52% of the theoretical capacity [=844 mAh (g-Cu)$^{-1}$].[42] The charge−discharge behavior of the silver and copper electrodes is consistent with the CV curves shown in Figure S2. A silver electrode shows peak current densities larger than 5 mA cm^{-2} for both oxidative (fluorination) and reductive (defluorination) processes at a scan rate of 10 mV s^{-1}. On the other hand, the copper electrode exhibits significantly lower CV current densities than the silver electrode despite having more than three times higher theoretical capacity than the silver electrode. A closer look into the charge−discharge curves obtained during cycling at the 0.1−1C current rates (Figure 1b) shows the silver electrode to have a polarization of less than 0.1 V, which is considerably lower than the case of copper-based positive electrodes.[41,42] These results confirm that the silver electrode has a significantly superior rate performance compared to the copper-based electrodes.

Although the capacity is observed to decline at current rates higher than 2C (Figure 1c), the silver electrode retains a reversible capacity of ca. 100 mAh (g-Ag)$^{-1}$ at the current rate of 10C (21st cycle). When the charge−discharge rate is reverted to 0.1C after the 27th cycle conducted at 50C rate, the discharge capacity recovers to ca. 230 mAh (g-Ag)$^{-1}$, denoting a capacity retention of 95% with respect to the first cycle. These results confirm that the silver electrode does not undergo significant degradation even during the high-rate charge−discharge cycles. Figure 1d compares the electrochemical performance of composite-type positive electrodes reported for room-temperature FSB operations.[23,25,29,41,42] The comparative results indicate that the present silver electrode has excellent compatibility with the FHIL electrolyte, given that previous studies could hardly facilitate charge−discharge measurements in the high-rate regions above 100 mA (g-active material)$^{-1}$.

The charge−discharge performance and rate capability of the silver electrode in the $[C_2C_1im][(FH)_{2.3}F]$ FHIL electrolyte was further investigated at 273 K to ascertain their compatibility at low temperatures, as shown in Figure S3. The $[C_2C_1im][(FH)_{2.3}F]$ FHIL has an ionic conductivity of 57.7 mS cm^{-1} at 273 K,[36] which is a markedly higher value than those reported for other FSB electrolytes at room temperature.[27,28,30,44] As can be seen in Figure S3a,b, the silver electrode confers relatively high discharge capacities of 226 and 209 mAh (g-Ag)$^{-1}$ at rates of 0.1C (third cycle) and 0.2C (sixth cycle), respectively, even at 273 K. These results are not significantly different from the results obtained during measurements at 298 K. Although the reversible capacity decreases with increasing charge−discharge rates, the polarization at the current rates of 0.5C and 1C is still minimal, indicative of no substantial performance degradation compared to the operation at 298 K (see also Figure 1b). Moreover, the discharge capacities are maintained at the 90−100 mAh (g-Ag)$^{-1}$ range, even at the current rate of 5C. Similar to the observations made at 298 K, the reversible capacity recovers when the current rate is reverted to 0.1C (28−30th cycles) after 50C rate operations, evincing that the electrode degradation caused by cycling at higher current rates is negligible even at lower temperatures (273 K). As shown in Figure S3c, battery operations at 273 K yield lower capacities than those at 298 K across the current rates investigated. At this juncture, it must be noted that the evaluation of FSB performance below room temperature has not been reported to date. As such, the present results show that silver electrodes alongside FHIL electrolytes can be a prospective electrochemical platform for achieving low-temperature (273 K) FSB operations.

Besides good rate performance, the durability of a battery is also a critical determinant for its deployment into practical operations. Therefore, to assess the durability of the FSB presented in this study, charge−discharge measurements of the silver electrode in the $[C_2C_1im][(FH)_{2.3}F]$ FHIL were performed for 100 cycles at 298 K at a current rate of 0.5C [=124 mA (g-Ag)$^{-1}$]. As illustrated in Figure 1e,f, the first cycle yielded a discharge capacity of 217 mAh (g-Ag)$^{-1}$, and a Coulombic efficiency of 97%. The capacity has slightly dropped to 209 mAh (g-Ag)$^{-1}$ after 10 cycles and continues to gradually decline throughout the cycling. However, the silver electrode maintains a discharge capacity of 196 mAh (g-Ag)$^{-1}$ even at the 100th cycle, which is commensurate to 79% of the theoretical capacity, and capacity retention of 90% compared to the first cycle. It is worth mentioning that the silver electrode maintains Coulombic efficiencies of almost 100% throughout the 100 cycles. Figure 1e shows that even though a slightly larger polarization is observed in the first charge curve, the charge−discharge curves are seen to overlap across the board, indicative of stable charge−discharge cycling throughout the 100 cycles. To the best of our knowledge, the remarkably high cycling stability observed in this study has not been reported for any other FSB positive electrode material. Additionally, in comparison to the poor capacity retention of less than 50% after 10 charge−discharge cycles previously reported for CuF_2 and copper metal electrodes in the FHIL electrolytes,[41,42] the silver positive electrode demonstrates exceptionally stable charge−discharge behavior, suggesting better eligibility for FSB applications.

For a clear perspective into the room-temperature energy storage properties of the FSB comprising the silver electrode in the $[C_2C_1im][(FH)_{2.3}F]$ FHIL, self-discharge tests were performed after fully charging the cells. First, the silver electrodes were fully charged to 1.1 V vs CuF_2/Cu at a current rate of 0.1C at 298 K and stored at an open-circuit potential for varying periods of time (1, 5, and 7 days). Subsequently, the electrodes were discharged at a current rate of 0.1C, and

https://doi.org/10.1021/acsaem.4c02021
ACS Appl. Energy Mater. 2025, 8, 108−121

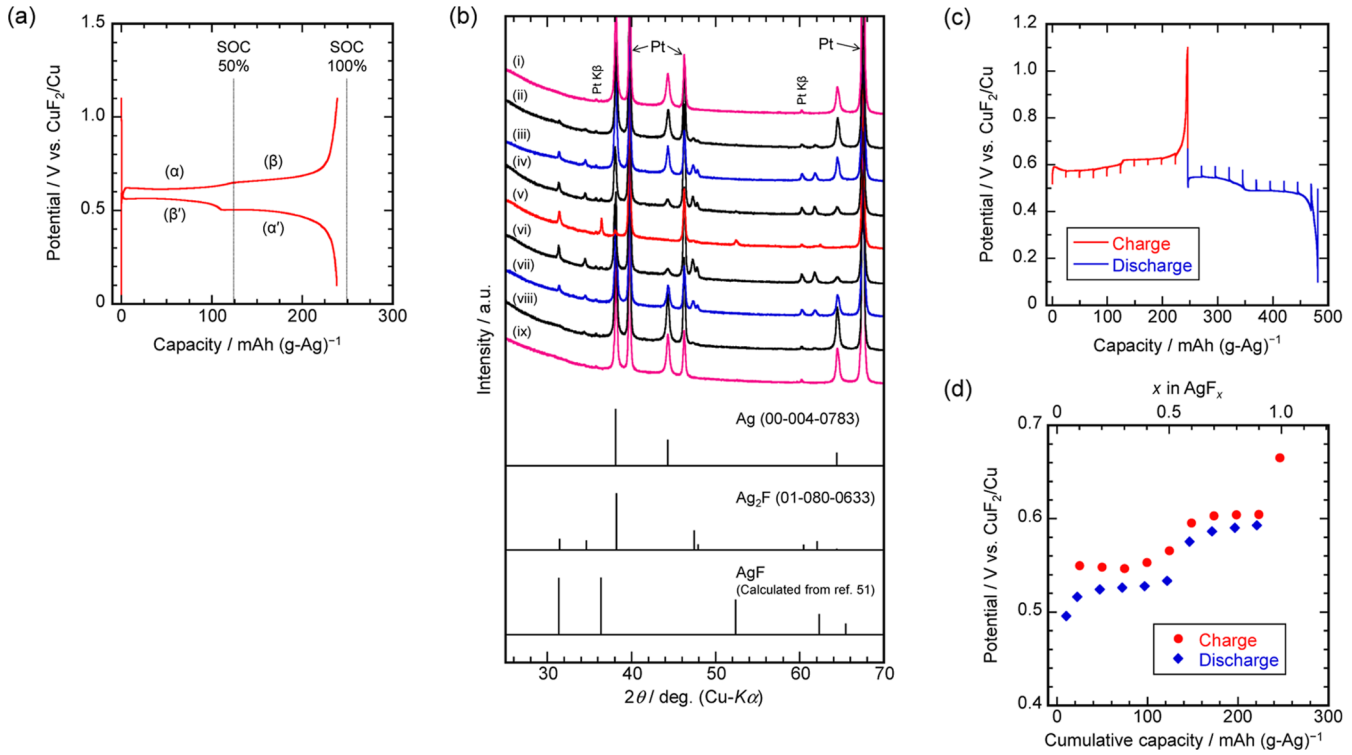

Figure 2. (a) Initial charge−discharge curves of a silver electrode (Ag: 150 nm) in the $[C_2C_1im][(FH)_{2.3}F]$ ionic liquid at 298 K. Charge−discharge current rate: 0.1C [=24.8 mA $(g\text{-}Ag)^{-1}$]. (b) Ex situ XRD patterns of silver electrodes (Ag: 150 nm) obtained during operations in the $[C_2C_1im][(FH)_{2.3}F]$ ionic liquid at 298 K at different charge−discharge states, i.e., (i) pristine state, (ii) 25%-charged state, (iii) 50%-charged state, (iv) 75%-charged state, (v) fully charged state, (vi) 25%-discharged state, (vii) 50%-discharged state, (viii) 75%-discharged state, and (ix) fully discharged state. Reference XRD patterns of the Ag, Ag_2F, and AgF are also provided. (c) GITT curves of a silver electrode (Ag: 150 nm), and (d) the resultant plots of relaxed open-circuit potentials with respect to fluorine compositions in $[C_2C_1im][(FH)_{2.3}F]$ ionic liquid at 298 K. The detailed conditions of GITT measurements are described in the experimental section.

the capacity retention ratios were calculated by dividing the discharge capacities by the charge capacities, as shown in Figure S4. The Coulombic efficiency of the first cycle, which was conducted at a current rate of 0.1C with no intervals between the charge and the discharge processes, was used as reference data for 0 day storage time. The capacity retention decreases slightly from 99.7% (0 day storage) to 99.0% after 1 day of storage. For the subsequent measurements, the capacity retention ratios are noted to decrease in a linear fashion, corresponding to the self-discharging rate of ca. 1% per day, eventually reaching 92% at the end of the 7 day storage period. Even though the capacity degradation observed here exceeds those of LIBs and state-of-the-art nickel-hydride metal (Ni-MH) batteries, it is still comparable to those observed in conventional Ni-MH batteries.[50] To date, self-discharge tests for FSBs have not been reported. Therefore, this study demonstrates, for the first time, the feasibility of FSB in terms of self-discharge characteristics.

3.2. Electrochemical Fluorination/Defluorination Mechanism of Silver. The electrochemical behavior of the silver positive electrode in the FHIL at 298 K was further investigated through charge−discharge tests performed at a current rate of 0.1C [=24.8 mA $(g\text{-}Ag)^{-1}$]. As shown in Figure 2a, the initial cycle attains charge and discharge capacities of 239 and 238 mAh $(g\text{-}Ag)^{-1}$, respectively, which are equivalent to 96% of the theoretical capacity [248 mAh $(g\text{-}Ag)^{-1}$]. The initial charge−discharge curves are characterized by two plateaus (denoted as plateaus α and β for charging and α' and β' for discharging) formed during both the charging and the discharge processes. The capacities of the plateaus α (α') and β (β') appear to be almost identical to each other [around 110−120 mAh $(g\text{-}Ag)^{-1}$], suggesting the existence of an intermediate compound at a composition of $x \approx 0.5$ in AgF_x.

For insight into the intermediate compounds formed in the silver positive electrodes during the charge and discharge processes in the FHIL at 298 K, ex-situ X-ray diffraction analyses were conducted on the positive electrodes at different charge−discharge states [i.e., (i) pristine state, (ii) 25%-charged, (iii) 50%-charged, (iv) 75%-charged, (v) fully charged, (vi) 25%-discharged, (vii) 50%-discharged, (viii) 75%-discharged, and (ix) fully discharged], as shown in Figure 2b. The patterns of Ag, Ag_2F, and AgF are also provided for reference. The AgF reference pattern was calculated from a previously reported crystal structure[51] using the RIETAN-FP system.[52] In the pristine state (i), several diffraction peaks from silver metal and the platinum current collector are detected, as should be expected. After charging to 25% of the theoretical capacity (ii), new diffraction peaks assignable to the Ag_2F phase appear at around 31.4°, 34.5°, 47.3°, 47.8°, 60.3°, and 61.8°. The silver metal peaks significantly decrease after charging to the 75%-charged state (iv), eventually disappearing at the full-charged state (v). In this state, the pattern associated with the Ag_2F phase almost vanishes, leaving behind the diffraction peaks assigned to the AgF phase at 31.4°, 36.4°, 52.4°, and 62.4°. The phase changes observed here are consistent with the charge−discharge profiles, i.e., the two plateaus of the same capacity observed during the charge process. In the discharge process (vi−ix), the Ag_2F phase

https://doi.org/10.1021/acsaem.4c02021
ACS Appl. Energy Mater. 2025, 8, 108−121

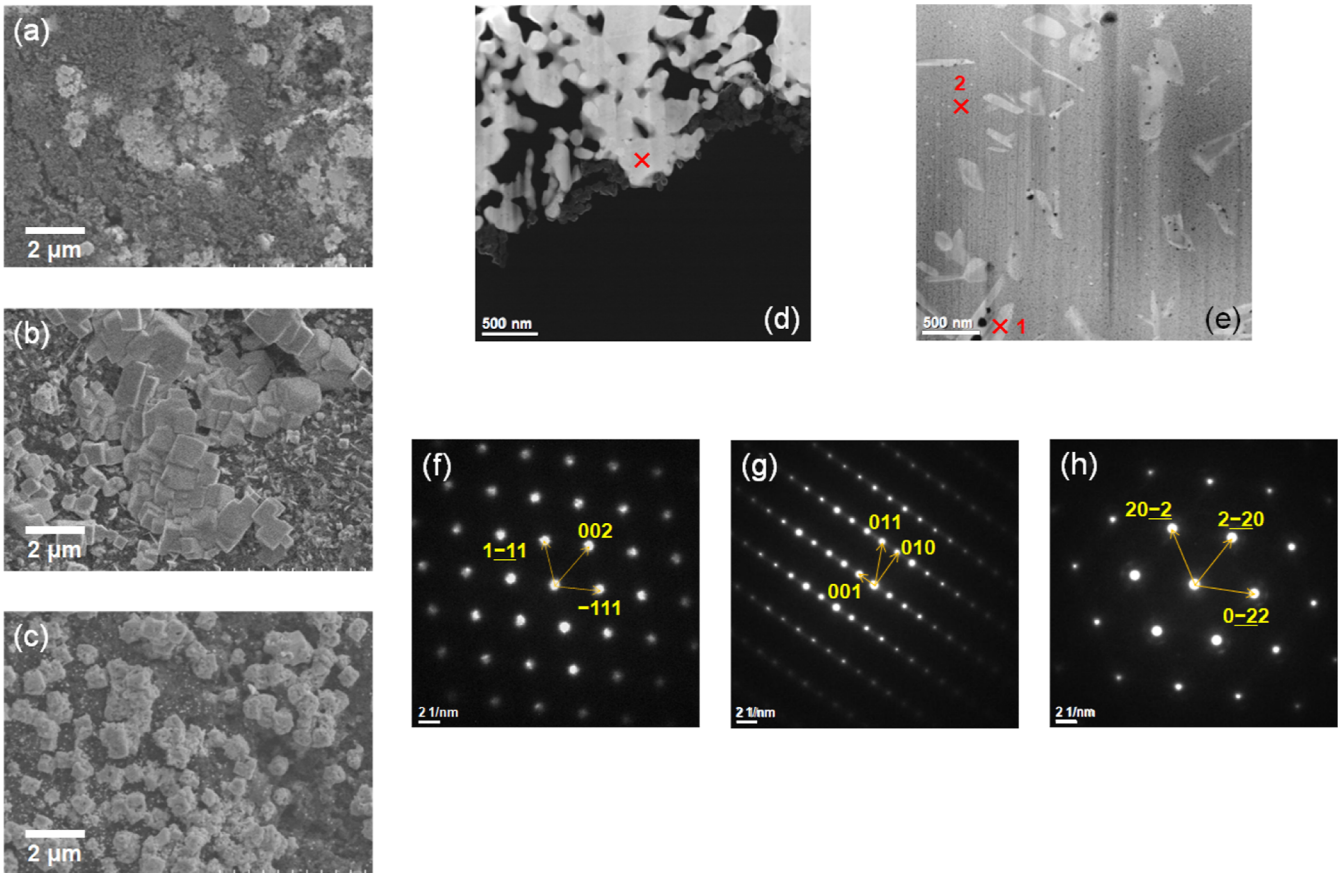

Figure 3. SEM images of (a) pristine, (b) full-charged, and (c) full-discharged silver electrodes, and TEM images of (d) pristine and (e) full-charged silver electrodes. (f) An electron diffraction (ED) pattern of the red cross point in the pristine electrode (Figure 3d). (g,h) ED patterns of points 1 and 2 in the full-charged electrode (Figure 3e), respectively. Initial silver particle size: 150 nm. The full-charged and full-discharged electrodes were prepared by operations in the $[C_2C_1im][(FH)_{2.3}F]$ ionic liquid at a current rate of 0.1C [=24.8 mA (g-Ag)$^{-1}$] at 298 K.

reappears at the 25%-discharged state and completely reverts to silver metal at the fully discharged state.

The X-ray diffraction results demonstrate the high reversibility of the reactions involving the silver electrode during the charge and discharge processes. The anionic species in the $[C_2C_1im][(FH)_{2.3}F]$ IL are $[(FH)_2F]^-$ and $[(FH)_3F]^-$ according to the previous work[37] and thus the redox reactions corresponding to the plateaus α (α') and β (β') are described as follows

$$(\alpha, \alpha')2Ag + 3[(FH)_2F]^- \rightleftharpoons Ag_2F + 2[(FH)_3F]^- + e^- \quad (3)$$

$$(\beta, \beta')Ag_2F + 3[(FH)_2F]^- \rightleftharpoons 2AgF + 2[(FH)_3F]^- + e^- \quad (4)$$

Although the anionic species may be other than $[(FH)_nF]^-$ (n = 2, 3), the fast HF exchange among the fluorohydrogenate ions confirmed in a previous work,[38] momentarily equilibrates the HF composition in the anionic species of the electrolyte. Even though the Ag_2F is well-known as a subfluoride,[53,54] its thermodynamic properties are still not well understood. Therefore, the galvanostatic intermittent titration technique (GITT) was conducted to confirm the equilibrium potentials of the reactions mentioned above (eqs 3 and 4), as shown in Figure 2c,d. As illustrated by the plots of relaxed open-circuit potentials versus the fluorine composition (x in AgF_x) in Figure 2d, potential plateaus emerge around 0.55 V in the compositional region of $0 < x < 0.5$ and at 0.60 V vs Cu/CuF_2 in the region of $0.5 < x < 1$, during both the charge and discharge processes. These plateaus are designated as the redox potentials of Ag_2F/Ag for $0 < x < 0.5$ and AgF/Ag_2F for $0.5 < x < 1$ expressed in eqs 3 and 4, respectively, in accordance with the results of XRD. Assuming the equilibrium potentials of Ag_2F/Ag and AgF/Ag_2F redox couples are 0.55 and 0.60 V, the standard Gibbs free energies of formation (ΔG_f^0) for Ag_2F and AgF phases at 298 K are determined to be −193 kJ (mol-Ag_2F)$^{-1}$ and −190 kJ (mol-AgF)$^{-1}$ through thermodynamic calculations. To our knowledge, this is the first time the ΔG_f^0 value of Ag_2F phase derived through electromotive force method is reported. Details of the thermodynamic calculations are provided in the Supporting Information. The GITT results further indicate that the polarization during discharge is visibly larger than the one during the charge process (Figure 2c). Although the reason for this difference is not clear at this stage, the complicated conversion reaction processes can be posited to engender distinct kinetics during the fluorination and defluorination processes. These mechanisms will be discussed in detail later in this report.

The concentrations and solubility of the active material in the electrolyte are known to influence the performance of FSBs.[23] The solubility of AgF in the FHIL electrolyte was investigated through ICP-AES analysis. At 298 K, the solubility of AgF in the $[C_2C_1im][(FH)_{2.3}F]$ FHIL was found to be ca. 200 ppm [=(mg-Ag) dm^{-3}]. When the volume of the electrolyte is 4×10^{-4} dm^3 per cell, the maximum mass of silver in certain ionic species formed by the chemical

https://doi.org/10.1021/acsaem.4c02021
ACS Appl. Energy Mater. 2025, 8, 108−121

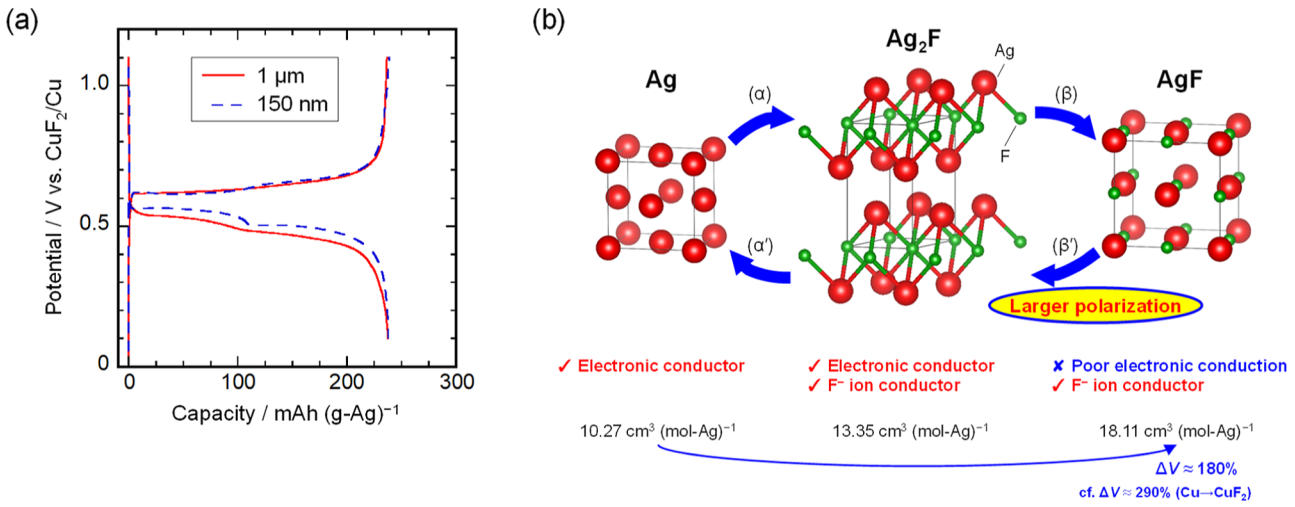

Figure 4. (a) Initial charge−discharge curves of silver electrodes comprising differently sized silver particles in the $[C_2C_1im][(FH)_{2.3}F]$ ionic liquid at 298 K. Charge−discharge current rate: 0.1C [=24.8 mA $(g\text{-}Ag)^{-1}$]. (b) A schematic illustration of fluorination/defluorination reactions of the silver electrode over one charge−discharge cycle. The crystal structures for Ag, Ag_2F, and AgF with their unit cells are also provided to show the structural changes occurring at each stage of the charge−discharge cycle. Here, the silver and fluorine atoms are portrayed as red and green spheres, respectively.

dissolution of AgF in the FHIL was determined to be 8×10^{-2} mg using the following equation

$$W_{Ag(sol)} = C_{Ag(ICP\text{-}AES)} \times V_{electrolyte} \quad (5)$$

where $W_{Ag(sol)}$ represents the mass of silver dissolved in the electrolyte (mg-Ag), $C_{Ag(ICP\text{-}AES)}$ is the concentration of silver determined by the ICP-AES analysis [(mg-Ag) dm^{-3}], and $V_{Electrolyte}$ denotes the volume of electrolyte in the electrochemical cell (dm^3). Given that the AgF can chemically dissolve into the $[C_2C_1im][(FH)_{2.3}F]$ FHIL, the electrochemical dissolution of silver metal may be assumed to occur, forming an ionic species of silver. Even so, it is difficult to detect the dissolved state of AgF due to its extremely low solubility. Therefore, we speculate that the $[AgF_2]^-$ complex ion may exist in the FHIL electrolyte, as previously reported.[55] Using the present case of the silver working electrode (Ag particle size: 150 nm) for the calculations in eq 5, no more than 5.3 wt % of the silver metal in the working electrode can be electrochemically dissolved into the electrolyte to form ionic species of silver because the amount of silver metal used in the working electrode is 1.5 mg per cell. During charge−discharge tests, the dissolved ionic species of silver is considered to exist under the equilibrium with AgF.

For an in-depth perspective into the origin of the outstanding performance exhibited by the silver positive electrode in the FHIL, the crystal evolutions of silver during the fluorination/defluorination processes in the first cycle were investigated by microscopic observation. As shown in the FE-SEM image of the pristine electrode (Figure 3a), silver is seen in brighter region as aggregates of fine particles in the 100−200 nm range. The particles are seen to grow during the charge process (Figure 3b), forming micrometer-sized cubes ascribed to AgF which belongs to a cubic crystal structure.[51] After the complete discharge (Figure 3c), the cubes shrink in size while retaining their structure, which is consistent with the observed XRD pattern of silver metal assigned to cubic crystal system. This unique microscopic crystal evolution is also supported by the results of TEM and electron diffraction (ED) analyses, as shown in Figure 3d−h. From an ED pattern of a particle in the pristine electrode, the d values were determined to be 2.37, 2.04, and 2.37 Å, which is assignable to the diffractions of silver metal as described in Table S2. Figure 3e shows the particle size of the active material become considerably larger after the electrode is fully charged. The particle observed consists of brighter needle-like regions and a darker bulk particle. These ED patterns indicate that Ag_2F locally exists in the AgF matrix.

From the interesting crystal growth behavior observed during the charge−discharge processes, it is natural to speculate that positive electrodes comprising larger silver particles can also be used for room-temperature FSBs. Thus, a silver composite electrode fabricated using 1 μm-sized silver particles was subjected to charge−discharge tests in the $[C_2C_1im][(FH)_{2.3}F]$ FHIL at 298 K. As shown in Figure S5a,b, the silver electrode with the larger particles delivers reversible capacities of approximately 240 mAh $(g\text{-}Ag)^{-1}$ at 0.1C rate, showing the two characteristic potential plateaus during both the charge and discharge processes. The electrode further maintains reasonably high capacities of around 200 mAh $(g\text{-}Ag)^{-1}$ even at 1C rate, evincing the extraordinary rate capability of large-sized active materials for room-temperature FSBs. Moreover, the electrode with the 1 μm-sized silver particles exhibits stable cycling for 50 cycles at the 0.5C rate (Figure S5c,d), proffering discharge capacities of more than 190 mAh $(g\text{-}Ag)^{-1}$ except during the first cycle. Figure S5e,f compare the charge−discharge performance of the two silver electrodes with different silver particles. Up to 1C rate operation, the composite electrode with the 1 μm-sized silver particles is seen to provide reversible (discharge) capacities comparable to the one with the 150 nm-sized particles. Likewise, the two composite electrodes display no significant differences in reversible capacities during cyclability tests conducted for 50 cycles at the current rate of 0.5C.

The influence of the active material particle sizes on the electrochemical behavior of the silver positive electrode in the FHIL electrolyte was further unraveled by comparing the initial charge−discharge curves obtained from the silver composite electrodes with differently sized active material particles. Figure 4a shows that both electrodes produce overlapping charging curves with no prominent differences in

https://doi.org/10.1021/acsaem.4c02021
ACS Appl. Energy Mater. 2025, 8, 108−121

their overpotentials during the fluorination reaction despite the large difference (more than 5 times) in their particle sizes. Even so, larger overpotentials are clearly observed for the silver electrode with 1 μm-sized silver particles during discharge (defluorination) process, which is consistent with the GITT results (See Figure 2c). Based on these results, it is necessary to consider the physical properties of the phases appearing during fluorination/defluorination reactions when exploring the underlying mechanisms.

Figure 4b illustrates a schematic drawing of the crystal structural evolutions occurring in the silver positive electrode (Ag, Ag_2F, and AgF phases) during the charge−discharge reactions as visualized by the VESTA system.[56] The starting material, i.e., silver metal, belongs to the $Fm\bar{3}m$ space group that comprises Ag layers with an ABC-type stacking [cubic close packing (ccp)] and a molar volume of 10.27 cm^3 $(mol\text{-}Ag)^{-1}$. The intermediate compound, Ag_2F, formed during the charge process, engenders a layered structure categorized into an anti-CdI_2 structure (Space group: $P\bar{3}m1$).[53,54] In this structure, the Ag layers transform into an AB-type stacking (hexagonal close packing) in which the F^- ions are intercalated between every other Ag layer where they occupy half of the octahedral sites and are coordinated by six Ag atoms. Since one Ag atom is bound to three F atoms, the bond valence sum (BVS) of Ag is determined to be 0.51 using the following equation[57]

$$\mathrm{BVS(Ag)} = \sum \exp\left(\frac{r_0 - r_i}{B}\right) \tag{6}$$

where r_0 denotes the bond valence parameter of Ag−F bond (1.80 Å[57]), r_i represents the Ag−F bond length in the Ag_2F structure (2.454 Å[54]), and B is an empirical constant (0.37 Å). Thus, the average valence of silver is determined to be +0.5, and the molar volume of Ag_2F is found to be 13.35 cm^3 $(mol\text{-}Ag)^{-1}$; 1.30 times larger than silver metal. At the fully charged state, the AgF adopts a NaCl-type cubic structure belonging to the same space group as silver metal ($Fm\bar{3}m$). The Ag layers revert to the ABC-type stacking (ccp) with F^- ions intercalated between all the Ag layers, occupying all the octahedral sites. The molar volume of AgF is determined to be 18.11 cm^3 $(mol\text{-}Ag)^{-1}$; 1.76 times larger than the molar volume of silver metal and 1.36 times that of Ag_2F. A list of molar volumes and volume expansion ratios of various metal positive electrodes during charging reaction is provided in Table S3. The volume expansion ratio of 1.76 during the evolution from Ag to AgF is comparable to other metal electrodes except for copper (2.9 for CuF_2/Cu).

AgF is known to be an excellent ionic conductor with an ionic conductivity of $\sim 4 \times 10^{-4}$ S cm^{-1} at 298 K,[58] which is much higher than those of CuF_2[10] and PbF_2.[9] Previous studies on band structures and conductivity measurements have shown Ag_2F to have metallic properties.[59−64] In fact, the Ag−Ag distance in Ag_2F is 2.81 Å, which is very close to that in silver metal (2.89 Å). Furthermore, since the Ag−F distance between Ag atoms in the Ag layer and the F atoms in the adjacent F layer in Ag_2F (2.45 Å) is close to that in AgF (2.47 Å), it is expected that the Ag−F bond in Ag_2F shows ionic nature,[62] and can therefore possibly facilitate ionic mobility. Accordingly, the excellent rate performance of the silver electrode can be explained by the existence of the so-called "mixed conductor matrix",[65,66] inclusive of electrical and ionic conducting materials. As summarized in Figure 4b, the charge and discharge processes begin with the electronic conductive silver metal and the F^- conductive AgF. Since AgF is considered to be a poor electronic conductor, the larger polarization observed during the discharge process can be associated with electronic conductivity rather than F^- conductivity. This hypothesis is consistent with the fact that silver electrodes with differently sized particles exhibit the overlapping charging curves with negligible differences in potential polarization, which can be ascribed to the high electronic conductivity of silver metal that hardly affects poor kinetics. This affirms that the charge−discharge performance of FSBs largely depends on the electronic conductivity of the active material as well as its F^- conductivity.

It should be noted that the fluorination/defluorination mechanism is very important for FSB studies. Konishi et al. first reported the mechanism of the dissolution and redeposition of active materials.[23] According to our previous studies on copper-based positive electrode materials in FHILs,[41,42] the dissolution and redeposition reactions affect their charge−discharge performance. AgF can be dissolved up to 200 ppm in $[C_2C_1im][(FH)_{2.3}F]$ FHIL, suggesting that the so-called dissolution and redeposition mechanism is involved in charge−discharge performance of the silver positive electrodes.

3.3. Other Feasible Fluorohydrogenate-Based Electrolytes for Room-Temperature FSBs. In an effort to broaden the variety of available electrolytes for room-temperature FSBs, another FHIL, $[C_2C_1pyrr][(FH)_{2.3}F]$, was employed as an FSB electrolyte alongside silver positive electrodes (initial silver particle size: 150 nm) at 298 K. The electrochemical performance of this configuration is provided in Figure S6. The silver electrode delivers charge−discharge capacities of over 220 mAh $(g\text{-}Ag)^{-1}$ during the rate capability measurements at 0.1C and 0.2C rates (Figure S6a,b). Although the reversible capacities are observed to decrease with increasing current rates, the silver electrode can still deliver nearly 50 mAh $(g\text{-}Ag)^{-1}$ at the high current rate of 10C. When the current rate is reverted to 0.1C after operation at the 50C rate, the capacity has recovered to approximately 230 mAh $(g\text{-}Ag)^{-1}$, indicating that the silver electrode suffers no significant degradation during the high-rate charge−discharge cycles. The cyclability measurements additionally reveal the silver electrode to be highly compatible with the $[C_2C_1pyrr][(FH)_{2.3}F]$ FHIL. As illustrated in Figure S6c,d, initial charge and discharge capacities at 0.1C-rate operation are 236 and 231 mAh $(g\text{-}Ag)^{-1}$, respectively, with characteristic two plateaus corresponding to Ag/Ag_2F and Ag_2F/AgF coexisting states. Although slightly larger potential polarization is observed in the first cycle, the subsequent charge−discharge curves are almost overlapped up to the 50th cycle. The discharge capacity at the 50th cycle is 227 mAh $(g\text{-}Ag)^{-1}$, which is commensurate with 98% capacity retention. This indicates that the silver metal electrode has an extremely high stability in this FHIL electrolyte. Similar cyclability tests were conducted at the 0.5C-rate, as shown in Figure S6e,f. At this current rate, the reversible capacities are maintained around 170 mAh $(g\text{-}Ag)^{-1}$ for 50 cycles with negligible changes in the charge−discharge curves. Figure S6g,h compare the silver electrode performance in the $[C_2C_1im][(FH)_{2.3}F]$ and $[C_2C_1pyrr][(FH)_{2.3}F]$ FHIL electrolytes. Although the reversible capacities in the two electrolytes are comparable at 0.1C and 0.2C rates, some differences in their performances are seen above 0.5C rate to manifest better rate capability for $[C_2C_1im][(FH)_{2.3}F]$ which is also consistent with the cyclability results at 0.5C rate. This

https://doi.org/10.1021/acsaem.4c02021
ACS Appl. Energy Mater. 2025, 8, 108−121

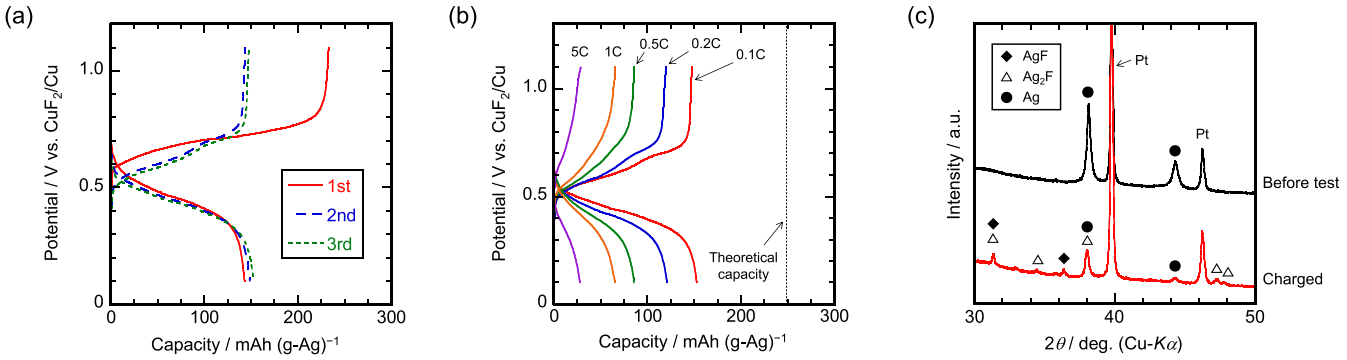

Figure 5. (a,b) Charge−discharge curves of a silver electrode (Ag: 150 nm) in the $[C_1C_1pyrr][(FH)_{1.9}F]$ ionic plastic crystal (IPC) electrolyte at 298 K. The silver composite electrode was prepared by the conventional impregnation method. Charge−discharge current rates: (a) 0.1C, (b) 0.1−5C. (c) Ex situ XRD patterns of the silver electrodes at pristine and full-charged states after 0.1C-rate operation in the IPC electrolyte at 298 K.

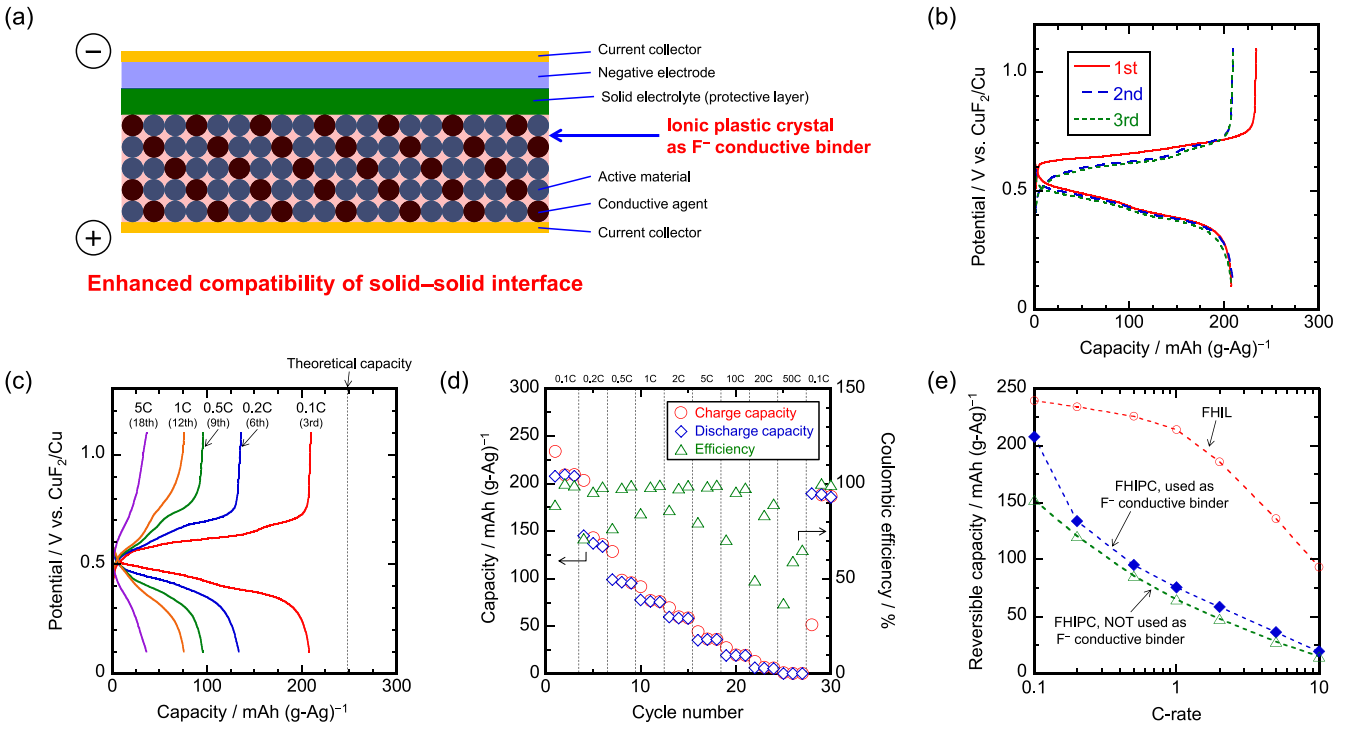

Figure 6. (a) A schematic illustration of a battery system with the IPC used as the F^- conductive binder, which is the target in the future. (b,c) Charge−discharge curves of a silver composite electrode (Ag: 150 nm) with the ionic plastic crystal (IPC) used as the F^- conductive binder in the $[C_1C_1pyrr][(FH)_{1.9}F]$ IPC electrolyte at 298 K. Charge−discharge current rates: (b) 0.1C, (c) 0.1−5C. (d) The cycling properties of the capacities and Coulombic efficiencies in the rate capability test. (e) Comparison of rate capability of silver electrodes in the FHIL ($[C_2C_1im][(FH)_{2.3}F]$) and the FHIPC ($[C_1C_1pyrr][(FH)_{1.9}F]$) electrolytes in the different configurations presented in this study.

observation can be ascribed to higher ionic conductivity of the $[C_2C_1im][(FH)_{2.3}F]$ FHIL at 298 K.[36,67]

In this pursuit of viable electrolyte alternatives to the FHIL, we focused on fluorohydrogenate ionic plastic crystals (FHIPCs) as promising candidates for developing safe FSBs. In general, ionic plastic crystals are considered to exhibit their excellent adhesion properties that allow the formation of robust electrode/electrolyte interfaces. In the present study, the $[C_1C_1pyrr][(FH)_{1.9}F]$ FHIPC was selected as an electrolyte for room-temperature FSBs because its melting point (338 K) and solid−solid phase transition point (251 K)[49] allow for operations over a wide temperature range. Additionally, $[C_1C_1pyrr][(FH)_{1.9}F]$ engenders an ionic conductivity of about 7 mS cm^{-1} at 298 K, marking its viability as an FSB electrolyte. As mentioned in the experimental section, we adopted two different methods for working electrode fabrication.

At first, a silver electrode was prepared by the conventional impregnation method, that is, in the same way as those used with the present liquid electrolytes except for the impregnation temperature which was raised to slightly above the FHIPC melting point (338 K). Prior to the measurements, the cell was stored at 323 K for 1 h to optimize the operation conditions. Figure 5a describes typical charge−discharge curves of a silver electrode (initial silver particle size: 150 nm) in $[C_1C_1pyrr][(FH)_{1.9}F]$ at 298 K. The initial charge and discharge capacities are found to be 233 and 143 mAh $(g\text{-}Ag)^{-1}$, respectively, at the current rate of 0.1C. The charge capacity seen here is comparable to those obtained from the present liquid electrolytes, while the discharge capacity is noticeably

https://doi.org/10.1021/acsaem.4c02021
ACS Appl. Energy Mater. 2025, 8, 108−121

lower, only achieving less than 60% of the theoretical capacity. From this observation, the utilization ratio of active materials in the charge process seems high enough. In addition, surface morphology of the silver electrodes was analyzed by FE-SEM observation before and after the initial charge process, as shown in Figure S7. As in the case of FHIL electrolyte (see also Figure 3b), the crystal growth is confirmed upon charging process, corresponding to the formation of silver fluorides. This significant morphological change might induce the reduction of adhesion property at the electrode/electrolyte interface. Therefore, the irreversible capacity can be attributed to the loss of electrical or ionic contact for a fraction of the active materials during charging, and not to the lower bulk ionic conductivity of the FHIPC compared to the liquid electrolytes. As shown in Figure 5b, the charge−discharge capacities gradually decrease with increasing current rates, although some reversible capacities are seen at rates higher than 1C. It is worth mentioning that these results represent the first reported performance of a composite electrode in the IPC electrolyte for room-temperature FSBs. Figure 5c illustrates XRD patterns of the silver composite electrode obtained before and after the initial charge process. Here, AgF and Ag_2F phases are formed with remaining small amount of silver metal, confirming that the present FHIPC electrolyte facilitates the fluorination reaction.

As a strategy for improving the reversible capacities of room-temperature FSBs, the present FHIPC was applied as not only electrolyte but also F^- conductive binder. Figure 6a illustrates the FSB configuration with the F^- conductive binder, which is the target in the future. Our previous studies of fuel cells have shown that the cathodic limit reaction involving fluorohydrogenate ions typically results in hydrogen gas evolution.[68] Thus, a protective layer such as solid electrolytes is required to prevent FHIPC decomposition, necessitating a two-layered solid electrolyte to develop an effective battery system that utilizes FHIPCs. This approach is presumed to enhance the compatibility at the solid−solid interface and is thus expected to provide a high utilization ratio of active materials. In the present study, silver electrodes were fabricated at room temperature by mixing the paste-like $[C_1C_1pyrr][(FH)_{1.9}F]$ FHIPC with other ingredients used for the liquid-electrolyte cells. For a streamlined production process, all procedures were performed at room temperature except for the electrolyte impregnation of separator which was done at elevated temperatures. The cells were also constructed at room temperature and the charge−discharge tests were conducted at 298 K without the cell warming steps.

Figure 6b shows the charge−discharge curves obtained from the silver composite electrode containing the $[C_1C_1pyrr][(FH)_{1.9}F]$ FHIPC used as the F^- conductive binder. The proposed battery system operated at 0.1C rate yields initial charge and discharge capacities of 234 and 208 mAh $(g\text{-}Ag)^{-1}$, respectively, providing a Coulombic efficiency of 88.8%. Additionally, the electrode is seen to maintain a capacity of approximately 210 mAh $(g\text{-}Ag)^{-1}$ for the initial three cycles. Compared to the silver electrode in the absence of the FHIPC (See Figure 5a), the discharge capacity is significantly improved while the charge capacity remains unchanged. This observation affirms that the addition of the FHIPC binder enhances the compatibility of the electrode and electrolyte at the interface. As shown in Figure 6c,d, the capacity decreases with increasing current rates, but it recovers to nearly 190 mAh $(g\text{-}Ag)^{-1}$ when the current rates are reverted to 0.1C rate after operation at 50C rate. These results are clear indicators of the viability of the FHIPC as FSB electrolytes. To probe the effect of F^- conductive binder, the electrochemical impedance spectroscopy (EIS) was conducted for cells just before charge−discharge tests. In this study, the spectra for the silver working electrode with respect to the AgF/Ag counter electrode was adopted due to the cell configuration. As shown in Figure S8, a large semicircle region was observed for the silver electrode without FHIPC as F^- conductive binder. In contrast, the silver electrode with FHIPC binder exhibited a reduced semicircle resistance, which indicates the improved electrical or ionic contact at the electrode/electrolyte interface and contributes the smaller polarization and higher reversible capacities. The cycling properties of the silver electrode containing the FHIPC were additionally investigated at the 0.5C rate for 50 cycles (Figure S9), indicating that the configuration can facilitate stable electrochemical behavior except for the gradual capacity decline observed in the initial 10 cycles. A comparison of the rate capability of the silver electrode in the presently discussed electrolyte systems is provided in Figure 6e. Here, the $[C_2C_1im][(FH)_{2.3}F]$ FHIL is seen to confer the highest FSB performance due to its extremely high ionic conductivity. However, the $[C_1C_1pyrr][(FH)_{1.9}F]$ FHIPC also shows admissible performance as an FSB electrolyte. In fact, the silver electrode made with the F^- conductive binder exhibits a rate performance superior to the conventional composite electrode.

4. CONCLUSIONS

In this study, we comprehensively investigated the viability of a silver positive electrode and the $[C_2C_1im][(FH)_{2.3}F]$ FHIL electrolyte for room-temperature fluoride shuttle batteries. The positive electrode yielded a high initial discharge capacity of 238 mAh $(g\text{-}Ag)^{-1}$ at the current rate of 0.1C, achieving a Coulombic efficiency of over 99.5%; commensurate with a 96% utilization of the theoretical capacity [248 mAh $(g\text{-}Ag)^{-1}$]. Ex situ XRD measurements performed on the electrode at different charge−discharge states revealed the formation of two silver fluoride phases, Ag_2F and AgF, via two-step reversible reactions during the electrochemical operations. Herein, we report for the first time the Gibbs free energy of formation for Ag_2F calculated via the electromotive force method. These thermodynamic calculations are expected to be instrumental in predicting the reaction potentials for future FSB electrolytes. Remarkably, the silver electrode working in the FHIL electrolyte not only exhibited significantly higher rate capability than previously proposed FSB positive electrodes at 298 K but also evidenced high electrochemical performance even at the lower temperature of 273 K. The excellent performance of this electrode was attributed to the formation of the so-called "mixed conductor matrix" engendered by the electronic and ionic conduction properties inherent in Ag_2F and AgF, respectively. The electrode's viability of long-term electrochemical operations was ascertained through a 100 charge−discharge cycling test conducted at a current rate of 0.5C and a series of self-discharge tests. The eligibility of the present silver electrode was further established in combination with other FSB electrolyte candidates, $[C_2C_1pyrr][(FH)_{2.3}F]$ FHIL and $[C_1C_1pyrr][(FH)_{1.9}F]$ FHIPC, which demonstrated relatively high performances at 298 K. Notably, the use of the FHIPC as both the F^- conductive binder and solid electrolyte for an FSB was found to improve the utilization ratio of active materials during operations, providing enhanced electro-

https://doi.org/10.1021/acsaem.4c02021
ACS Appl. Energy Mater. 2025, 8, 108−121

chemical performance. Further, we propose a streamlined production process of FSBs where silver electrodes were fabricated by mixing the FHIPC with other precursors at room temperature, eliminating the electrolyte impregnation steps that require elevated temperatures. This study not only presents silver metal as an auspicious active material for FSB positive electrodes in room-temperature operations but also aims to provide valuable insights that are bound to propel the development of high-performance FSBs.

■ ASSOCIATED CONTENT

Supporting Information

The Supporting Information is available free of charge at https://pubs.acs.org/doi/10.1021/acsaem.4c02021.

Summary tables for positive electrode materials of FSBs and the results of electron diffraction; Supporting figures of the CV comparison, rate performance at 273 K, self-discharge tests, charge−discharge tests using the electrode with larger-sized silver particles, charge−discharge tests using $[C_2C_1pyrr][(FH)_{2.3}F]$ FHIL and $[C_1C_1pyrr][(FH)_{1.9}F]$ FHIPC, SEM−EDX analysis, and impedance spectroscopy; Thermodynamic calculation procedures (PDF)

■ AUTHOR INFORMATION

Corresponding Authors

Takayuki Yamamoto − *Institute of Advanced Energy, Kyoto University, Kyoto 611-0011, Japan;* orcid.org/0000-0003-3553-3272; Phone: + 81-774-38-3510; Email: yamamoto.takayuki.2w@kyoto-u.ac.jp; Fax: +81-774-38-3499

Toshiyuki Nohira − *Institute of Advanced Energy, Kyoto University, Kyoto 611-0011, Japan;* orcid.org/0000-0002-4053-554X; Phone: + 81-774-38-3500; Email: nohira.toshiyuki.8r@kyoto-u.ac.jp; Fax: +81-774-38-3499

Authors

Kazuhiko Matsumoto − *Graduate School of Energy Science, Kyoto University, Kyoto 606-8501, Japan;* orcid.org/0000-0002-0770-9210

Rika Hagiwara − *Graduate School of Energy Science, Kyoto University, Kyoto 606-8501, Japan*

Complete contact information is available at: https://pubs.acs.org/10.1021/acsaem.4c02021

Notes

The authors declare no competing financial interest.

■ ACKNOWLEDGMENTS

This study is based on results obtained from projects, "Research and Development Initiative for Scientific Innovation of New Generation Batteries 2 and 3 (RISING2 and RISING3)", commissioned by the New Energy and Industrial Technology Development Organization (NEDO), Japan (Project codes: JPNP16001 and JPNP21006).

■ REFERENCES

(1) Whittingham, M. S. Ultimate Limits to Intercalation Reactions for Lithium Batteries. *Chem. Rev.* **2014**, *114*, 11414−11443.

(2) Cheng, F.; Chen, J. Metal−air batteries: from oxygen reduction electrochemistry to cathode catalysts. *Chem. Soc. Rev.* **2012**, *41*, 2172−2192.

(3) Fu, J.; Cano, Z. P.; Park, M. G.; Yu, A.; Fowler, M.; Chen, Z. Electrically Rechargeable Zinc−Air Batteries: Progress, Challenges, and Perspectives. *Adv. Mater.* **2017**, *29*, 1604685.

(4) Yoo, H. D.; Shterenberg, I.; Gofer, Y.; Gershinsky, G.; Pour, N.; Aurbach, D. Mg rechargeable batteries: an on-going challenge. *Energy Environ. Sci.* **2013**, *6*, 2265−2279.

(5) Stievano, L.; Meatza, I.; Bitenc, J.; Cavallo, C.; Brutti, S.; Navarra, M. A. Emerging calcium batteries. *J. Power Sources* **2021**, *482*, 228875.

(6) Anji Reddy, M.; Fichtner, M. Batteries based on fluoride shuttle. *J. Mater. Chem.* **2011**, *21*, 17059.

(7) Gschwind, F.; Rodriguez-Garcia, G.; Sandbeck, D. J. S.; Gross, A.; Weil, M.; Fichtner, M.; Hörmann, N. Fluoride ion batteries: Theoretical performance, safety, toxicity, and a combinatorial screening of new electrodes. *J. Fluorine Chem.* **2016**, *182*, 76−90.

(8) Nowroozi, M. A.; Mohammad, I.; Molaiyan, P.; Wissel, K.; Munnangi, A. R.; Clemens, O. Fluoride ion batteries − past, present, and future. *J. Mater. Chem. A* **2021**, *9*, 5980−6012.

(9) Kennedy, J. H.; Miles, R.; Hunter, J. Solid Electrolyte Properties and Crystal Forms of Lead Fluoride. *J. Electrochem. Soc.* **1973**, *120*, 1441−1446.

(10) Kennedy, J. H.; Hunter, J. C. Thin-Film Galvanic Cell Pb/PbF_2/PbF_2,CuF_2/Cu. *J. Electrochem. Soc.* **1976**, *123*, 10−14.

(11) Kennedy, J. H.; Miles, R. C. Ionic Conductivity of Doped Beta-Lead Fluoride. *J. Electrochem. Soc.* **1976**, *123*, 47−51.

(12) Schoonman, J. A Solid-State Galvanic Cell with Fluoride-Conducting Electrolytes. *J. Electrochem. Soc.* **1976**, *123*, 1772−1775.

(13) Danto, Y.; Poujade, G.; Pistré, J. D.; Lucat, C.; Salardenne, J. A. Pb|PbF_2|BiF_3|Bi Thin Solid Film Reversible Galvanic Cell. *Thin Solid Films* **1978**, *55*, 347−354.

(14) Schoonman, J.; Wolfert, A. Solid-State Galvanic Cells with Fast Fluoride Conducting Electrolytes. *Solid State Ionics* **1981**, *3*−*4*, 373−379.

(15) Rongeat, C.; Anji Reddy, M.; Diemant, T.; Behm, R. J.; Fichtner, M. Development of new anode composite materials for fluoride ion batteries. *J. Mater. Chem. A* **2014**, *2*, 20861−20872.

(16) Grenier, A.; Gutierrez, A. G. P.; Groult, H.; Dambournet, D. Modified coin cells to evaluate the electrochemical properties of solid-state fluoride-ion batteries at 150°C. *J. Fluorine Chem.* **2016**, *191*, 23.

(17) Thieu, D. T.; Fawey, M. H.; Bhatia, H.; Diemant, T.; Chakravadhanula, V. S. K.; Behm, R. J.; Kübel, C.; Fichtner, M. CuF_2 as Reversible Cathode for Fluoride Ion Batteries. *Adv. Funct. Mater.* **2017**, *27*, 1701051.

(18) Nowroozi, M. A.; Wissel, K.; Rohrer, J.; Munnangi, A. R.; Clemens, O. $LaSrMnO_4$: Reversible Electrochemical Intercalation of Fluoride Ions in the Context of Fluoride Ion Batteries. *Chem. Mater.* **2017**, *29*, 3441−3453.

(19) Nowroozi, M. A.; Ivlev, S.; Rohrer, J.; Clemens, O. La_2CoO_4: a new intercalation based cathode material for fluoride ion batteries with improved cycling stability. *J. Mater. Chem. A* **2018**, *6*, 4658−4669.

(20) Mohammad, I.; Witter, R.; Fichtner, M.; Anji Reddy, M. Room-Temperature, Rechargeable Solid-State Fluoride-Ion Batteries. *ACS Appl. Energy Mater.* **2018**, *1*, 4766−4775.

(21) Nakano, H.; Matsunaga, T.; Mori, T.; Nakanishi, K.; Morita, Y.; Ide, K.; Okazaki, K.; Orikasa, Y.; Minato, T.; Yamamoto, K.; Ogumi, Z.; Uchimoto, Y. Fluoride-Ion Shuttle Battery with High Volumetric Energy Density. *Chem. Mater.* **2021**, *33*, 459−466.

(22) Gschwind, F.; Zao-Karger, Z.; Fichtner, M. A fluoride-doped PEG matrix as an electrolyte for anion transportation in a room-temperature fluoride ion battery. *J. Mater. Chem. A* **2014**, *2*, 1214−1218.

(23) Konishi, H.; Minato, T.; Abe, T.; Ogumi, Z. Electrochemical Performance of a Bismuth Fluoride Electrode in a Reserve-Type Fluoride Shuttle Battery. *J. Electrochem. Soc.* **2017**, *164*, A3702−A3708.

(24) Konishi, H.; Kucuk, A. C.; Minato, T.; Abe, T.; Ogumi, Z. Improved electrochemical performances in a bismuth fluoride electrode prepared using a high energy ball mill with carbon for fluoride shuttle batteries. *J. Electroanal. Chem.* **2019**, *839*, 173−176.
(25) Konishi, H.; Minato, T.; Abe, T.; Ogumi, Z. Charge and Discharge Reactions of a Lead Fluoride Electrode in a Liquid-Based Electrolyte for Fluoride Shuttle Batteries:-The Role of Triphenylborane as an Anion Acceptor-. *ChemistrySelect* **2019**, *4*, 5984−5987.
(26) Yamanaka, T.; Okazaki, K.; Ogumi, Z.; Abe, T. Reactivity and Mechanisms in Fluoride Shuttle Battery Reactions: Difference between Orthorhombic and Cubic BiF_3 Single Microparticles. *ACS Appl. Energy Mater.* **2019**, *2*, 8801−8808.
(27) Okazaki, K.; Uchimoto, Y.; Abe, T.; Ogumi, Z. Charge−Discharge Behavior of Bismuth in a Liquid Electrolyte for Rechargeable Batteries Based on a Fluoride Shuttle. *ACS Energy Lett.* **2017**, *2*, 1460−1464.
(28) Davis, V. K.; Bates, C. M.; Omichi, K.; Savoie, B. M.; Momčilović, N.; Xu, Q.; Wolf, W. J.; Webb, M. A.; Billings, K. J.; Chou, N. H.; Alayoglu, S.; McKenney, R. K.; Darolles, I. M.; Nair, N. G.; Hightower, A.; Rosenberg, D.; Ahmed, M.; Brooks, C. J.; Miller III, T. F.; Grubbs, R. H.; Jones, S. C. Room-temperature cycling of metal fluoride electrodes: Liquid electrolytes for high-energy fluoride ion cells. *Science* **2018**, *362*, 1144−1148.
(29) Celik Kucuk, A.; Yamanaka, T.; Minato, T.; Abe, T. Influence of LiBOB as an Electrolyte Additive on the Performance of BiF_3/C for Fluoride Shuttle Batteries. *J. Electrochem. Soc.* **2020**, *167*, 120508.
(30) Celik Kucuk, A.; Abe, T. Borolan-2-yl involving anion acceptors for organic liquid electrolyte-based fluoride shuttle batteries. *J. Fluorine Chem.* **2020**, *240*, 109672.
(31) Alshangiti, O.; Galatolo, G.; Rees, G. J.; Guo, H.; Quirk, J. A.; Dawson, J. A.; Pasta, M. Solvent-in-Salt Electrolytes for Fluoride Ion Batteries. *ACS Energy Lett.* **2023**, *8*, 2668−2673.
(32) Zou, P.; Wang, C.; He, Y.; Xin, H. L.; Lin, R. A Water-in-Salt Electrolyte for Room-Temperature Fluoride-Ion Batteries Based on a Hydrophobic−Hydrophilic Salt. *Nano Lett.* **2024**, *24*, 5429−5435.
(33) Yu, Y.; Lin, A.; Lei, M.; Lai, C.; Wu, C.; Sun, Y.-Y.; Li, C. High-Capacity and Long-Cycling F-Ion Pouch Cells Enabled by Green Electrolytes. *ACS Energy Lett.* **2024**, *9*, 1008−1016.
(34) Li, G.; Yu, Y.; Li, D.; Li, C. Electrolyte Design by Synergistic High-Donor Solvent and Alcohol Anion Acceptor for Reversible Fluoride Ion Batteries. *Adv. Funct. Mater.* **2024**, *34*, 2406421.
(35) Hagiwara, R.; Hirashige, T.; Tsuda, T.; Ito, Y. Acidic 1-ethyl-3-methylimidazolium fluoride: a new room temperature ionic liquid. *J. Fluorine Chem.* **1999**, *99*, 1−3.
(36) Hagiwara, R.; Hirashige, T.; Tsuda, T.; Ito, Y. A Highly Conductive Room Temperature Molten Fluoride: EMIF·2.3HF. *J. Electrochem. Soc.* **2002**, *149*, D1−D6.
(37) Hagiwara, R.; Nakamori, Y.; Matsumoto, K.; Ito, Y. The Effect of the Anion Fraction on the Physicochemical Properties of $EMIm(HF)_nF$ (n = 1.0−2.6). *J. Phys. Chem. B* **2005**, *109*, 5445−5449.
(38) Enomoto, T.; Nakamori, Y.; Matsumoto, K.; Hagiwara, R. Ion−Ion Interactions and Conduction Mechanism of Highly Conductive Fluorohydrogenate Ionic Liquids. *J. Phys. Chem. C* **2011**, *115*, 4324−4332.
(39) Saito, Y.; Hirai, K.; Matsumoto, K.; Hagiwara, R.; Minamizaki, Y. Ionization State and Ion Migration Mechanism of Room Temperature Molten Dialkylimidazolium Fluorohydrogenates. *J. Phys. Chem. B* **2005**, *109*, 2942−2948.
(40) Taniki, R.; Matsumoto, K.; Nohira, T.; Hagiwara, R. Evaluation of Double-Layer and Redox Capacitances of Activated Carbon Electrodes in *N*-Ethyl-*N*-methylpyrrolidinium Fluorohydrogenate Ionic Liquid. *J. Electrochem. Soc.* **2013**, *160*, A734−A738.
(41) Yamamoto, T.; Matsumoto, K.; Hagiwara, R.; Nohira, T. Room-Temperature Fluoride Shuttle Batteries Based on a Fluorohydrogenate Ionic Liquid Electrolyte. *ACS Appl. Energy Mater.* **2019**, *2*, 6153−6157.
(42) Yamamoto, T.; Matsumoto, K.; Hagiwara, R.; Nohira, T. Charge−Discharge Performance of Copper Metal Positive Electrodes in Fluorohydrogenate Ionic Liquids for Fluoride-shuttle Batteries. *J. Electrochem. Soc.* **2021**, *168*, 040530.
(43) Barin, I. *Thermochemical Data of Pure Substances*; Wiley VCH: Weinheim, Germany, 1989.
(44) Kawasaki, M.; Morigaki, K.; Kano, G.; Nakamoto, H.; Takekawa, R.; Kawamura, J.; Minato, T.; Abe, T.; Ogumi, Z. Lactone-Based Liquid Electrolytes for Fluoride Shuttle Batteries. *J. Electrochem. Soc.* **2021**, *168*, 010529.
(45) Yokoyama, Y.; Kano, K.; Kondo, Y.; Miyahara, Y.; Miyazaki, K.; Abe, T. Fluoride Ion-Selective Electrode for Organic Solutions. *Anal. Chem.* **2021**, *93*, 15058−15062.
(46) Hwang, J.; Yamamoto, T.; Sakuda, A.; Matsumoto, K.; Miyazaki, K. Electrode Potentials Part 2: Nonaqueous and Solid-State Systems. *Electrochemistry* **2022**, *90*, 102002.
(47) Taniki, R.; Matsumoto, K.; Nohira, T.; Hagiwara, R. All solid-state electrochemical capacitors using *N,N*-dimethylpyrrolidinium fluorohydrogenate as ionic plastic crystal electrolyte. *J. Power Sources* **2014**, *245*, 758−763.
(48) Taniki, R.; Matsumoto, K.; Hagiwara, R.; Hachiya, K.; Morinaga, T.; Sato, T. Highly Conductive Plastic Crystals Based on Fluorohydrogenate Anions. *J. Phys. Chem. B* **2013**, *117*, 955−960.
(49) Taniki, R.; Matsumoto, K.; Hagiwara, R. Effects of HF content in the $(FH)_nF^-$ anion on the formation of ionic plastic crystal phases of *N*-ethyl-*N*-methylpyrrolidinium and *N,N*-dimethylpyrrolidinium fluorohydrogenate salts. *Phys. Chem. Chem. Phys.* **2014**, *16*, 1522−1528.
(50) Zhu, W. H.; Zhu, Y.; Davis, Z.; Tatarchuk, B. J. Energy efficiency and capacity retention of Ni−MH batteries for storage applications. *Appl. Energy* **2013**, *106*, 307−313.
(51) Bottger, G. L.; Geddes, A. L. Lattice Vibrations, Crystal Structure, Dielectric Properties, and Elastic Constants of AgF. *J. Chem. Phys.* **1972**, *56*, 3735−3739.
(52) Izumi, F.; Momma, K. Three-dimensional Visualization in Powder Diffraction. *Solid State Phenom.* **2007**, *130*, 15−20.
(53) Terrey, H.; Diamond, H. The crystal structure of silver subfluoride. *J. Chem. Soc.* **1928**, 2820−2824.
(54) Williams, A. Neutron powder diffraction study of silver subfluoride. *J. Phys.: Condens. Matter* **1989**, *1*, 2569−2574.
(55) Corcos, A. R.; Berry, J. F. Capturing the missing $[AgF_2]^-$ anion within an Ru_2(III/III) dimeric dumbbell complex. *Dalton Trans.* **2016**, *45*, 2386−2389.
(56) Momma, K.; Izumi, F. VESTA 3 for three-dimensional visualization of crystal, volumetric and morphology data. *J. Appl. Crystallogr.* **2011**, *44*, 1272−1276.
(57) Brese, N. E.; O'Keeffe, M. Bond-Valence Parameters for Solids. *Acta Crystallogr., Sect. B:Struct. Sci.* **1991**, *B47*, 192−197.
(58) Raaen, A. M.; Svare, I.; Fjeldly, T. A. Diffusion in silver fluoride. *Phys. Chem. B* **1980**, *21*, 4895−4897.
(59) Hilsch, R.; Minnigerode, G. V.; Wartenberg, H. V. Elektrische Leitfähigkeit von Ag_2F und ihre Temperaturabhängigkeit. *Naturwissenschaften* **1957**, *44*, 463−464.
(60) Kawamura, H.; Shirotani, I.; Inokuchi, H. Electrical Conductivity in Ag_2F Single Crystals. *Chem. Phys. Lett.* **1974**, *24*, 549−550.
(61) Hamada, N.; Ido, S.; Kitazawa, K.; Tanaka, S. Band structure of Ag_2F. *J. Phys. C: Solid State Phys.* **1986**, *19*, 1355−1362.
(62) Sun, F.; Takahashi, T.; Takakuwa, Y.; Yaegashi, H.; Sagawa, T. Photoemission study of quasi-two dimensional metal; Ag_2F. *J. Phys. Soc. Jpn.* **1986**, *55*, 461−464.
(63) Wang, X.; Ikezawa, M. Anisotropic Drude Reflectivity of Ag_2F Crystal. *J. Phys. Soc. Jpn.* **1991**, *60*, 1398−1405.
(64) Tong, W.; Amatucci, G. G. Mechanochemical synthesis of metallic Ag_2F and application to $Ag_3MoO_3F_3$ based nanocomposites for lithium batteries. *J. Power Sources* **2011**, *196*, 1449−1454.
(65) Boukamp, B. A.; Lesh, G. C.; Huggins, R. A. All-Solid Lithium Electrodes with Mixed-Conductor Matrix. *J. Electrochem. Soc.* **1981**, *128*, 725−729.

https://doi.org/10.1021/acsaem.4c02021
ACS Appl. Energy Mater. 2025, 8, 108−121

(66) Anani, A. A.; Crouch-Baker, S.; Huggins, R. A. Investigation of a Ternary Lithium Alloy Mixed-Conducting Matrix Electrode at Ambient Temperature. *J. Electrochem. Soc.* **1988**, *135*, 2103−2105.
(67) Matsumoto, K.; Hagiwara, R.; Ito, Y. Room-Temperature Ionic Liquids with High Conductivities and Wide Electrochemical Windows. *Electrochem. Solid-State Lett.* **2004**, *7*, No. E41.
(68) Hagiwara, R.; Nohira, T.; Matsumoto, K.; Tamba, Y. A Fluorohydrogenate Ionic Liquid Fuel Cell Operating Without Humidification. *Electrochem. Solid-State Lett.* **2005**, *8*, A231.

https://doi.org/10.1021/acsaem.4c02021
ACS Appl. Energy Mater. 2025, 8, 108−121